Analysis of induced-charge electro-osmotic flow in a microchannel embedded with polarizable dielectric blocks

Cunlu Zhao and Chun Yang*
School of Mechanical and Aerospace Engineering, Nanyang Technological University, 50 Nanyang Avenue, Singapore 639798, Republic of Singapore
(Received 30 May 2009; published 15 October 2009)

Within the frame work of classic electromagnetic theory, a general electrical boundary condition describing the induced-charge electrokinetic phenomena at the liquid-dielectric interface is proposed in the present study. Two well-known limiting cases, i.e., perfectly insulating and perfectly polarizable wall boundary conditions, can be recovered from the present electrical boundary condition. By utilizing the proposed boundary condition, the induced-charge electro-osmosis (ICEO) flow in an infinitely long microchannel patterned with two symmetric polarizable dielectric blocks is investigated analytically. Fourier transform method is invoked to solve a biharmonic equation, which governs the (ICEO) flow field described by the stream function. Dimensionless parameters are introduced, and their effects on flow characteristics are analyzed. It is found that an increase in polarizability of the dielectric block enhances the slip velocity on its surface and thus induces a pair of counter-rotating vortices. Also, increasing the natural zeta potential on the upstream and downstream of the insulating microchannel walls leads to extinction of the vortex near the upstream insulating microchannel and suppression of the vortex near the downstream insulating microchannel.

DOI: 10.1103/PhysRevE.80.046312 PACS number(s): 47.57.jd, 47.65.−d, 47.85.L−, 47.61.Fg

I. INTRODUCTION

Electrokinetics, including electro-osmosis, electrophoresis, and dielectrophoresis, plays an important role in manipulation of liquid flow and particles in microfluidic contexts. General description of electrokinetic flows in microfluidic channels with thin electric double layer (EDL) utilizes a slip velocity approximate approach to avoid the need of solving the detailed profiles of the EDL potential and fluid velocity. Such slip velocity can be described by the Helmholtz-Smoluchowski equation ($V_s=-\varepsilon\zeta E/\mu$), which is associated with the electric permittivity ε and dynamic viscosity μ of the liquid, the applied local electric field E, and the zeta potential of the channel wall ζ, thereby providing an appropriate boundary condition for the hydrodynamic problems in microfluidics. For a uniform prescribed zeta potential, the resulting flow is irrotational [1]. Nonetheless, the preceding description is adequate for perfectly insulating channel surfaces that usually bear natural electric charges (or natural zeta potential). On the other hand, electrokinetic flows can also be generated around a conducting body. Such flows, however, are driven by induced electrical charges due to electrical polarization mechanisms under effect of applied electric field. Although the induced electric charges are also situated on the surface of conducting objects, they are not the result of any physicochemical mechanisms (e.g., natural zeta potential), but rather a simple consequence of the Gauss law. Moreover, these charges distribute over the conductor surfaces so as to assure zero electric field in conductor interior. The resulting dependence of the surface charge density (and consequently the ζ potential) upon externally applied field strength gives rise to a nonlinear Helmholtz-Smoluchowski relation for the slip velocity. Flows driven by this induced electrokinetic mechanism, engendered by both dc and ac external fields, were initially discussed mainly among the colloid community in the Ukrainian literature [2–4]. Recently, Squires and Bazant [5] revisited the induced-charge electrokinetics and explored its relation to widely studied nonlinear electrokinetic phenomena, e.g., ac electro-osmosis [6,7]. Squires and Bazant [5] coined the terms "induced-charge electro-osmosis" (ICEO) and "induced-charge electrophoresis" (ICEP) to respectively describe the associated fluid and particle motion. They also suggested using ICEO generated by conducting elements of asymmetric shapes to perform a variety of microfluidic operations, such as pumping, mixing, and particle manipulations. Experimental verifications of these ICEO and ICEP effects were recently reported [8–10].

Numerous studies have been reported on the application of induced-charge electrokinetic (ICEK) phenomena in microfluidics. Bazant and Ben [11] proposed some new design principles for periodic three-dimensional ac electro-osmotic pumps based on the concept of ICEO, one of the most effective is the creation of fluid conveyor belt of ICEO flow over a stepped electrode array. Yariv [12] theoretically analyzed the ICEP motion of nonspherical particles, and found that nonspherical particles may translate and/or rotate in response to an imposed electric field, even if the net electric charges on particles vanish. Saintillan *et al.* [13] reported a study of the behavior of dispersed conducting slender rods in an electric field. In particular, they showed that the nonlinear induced-charge electrophoretic motion can be modeled by a linear slip velocity along the rod axes, which causes the alignment of the rods in the direction of the electric field and induces linear distributions of point-force singularities. These distributions of point forces drive stresslet disturbance flows in the surrounding fluid, resulting in hydrodynamic interactions. Leinweber *et al.* [14] realized a continuous microfluidic demixing process which utilizes high external

*Author to whom correspondence should be addressed. FAX: (+65) 6792-4062; mcyang@ntu.edu.sg

electrical fields that are applied over electrically floating noble metal electrodes. It is shown that a homogeneously concentrated electrolyte was successfully separated into arbitrarily shaped laminae of increased and depleted concentrations by this microfluidic demixer. Harnett *et al.* [15] designed a mixer for microfluidic sample preparation, where ICEO is adopted to create microvortices in a fluidic microchannel by application of an alternating current electric field. It is demonstrated that their proposed mixing scheme does not suffer from sample dilution, and thus preserves detection sensitivity. Wu and Li [16] proposed a correction method to estimate the induced zeta potential on conducting surfaces. They further conducted both experimental and numerical studies of the mixing enhancement in a polydimethylsiloxane (PDMS) microchannel with aid of ICEO generated by patterned platinum conducting hurdles.

Above cited analyses of ICEO or ICEP mostly focus on perfectly conducting surfaces or particles. The only exceptional case is the study reported by Squires and Bazant [5] who considered reduction in induced zeta potential due to a thin dielectric coating on a conducting cylinder. However, they assumed that the electric field strength does not vary inside the thin dielectric coating. Of more general interest, solid objects cannot be treated as either perfectly conducting or completely insulating [17]. When dealing with electrokinetic phenomena on a solid object surface with finite dielectric constant (rather than a perfectly conducting or completely insulating object surface), electrical potential distributions inside such polarizable dielectric object should be taken into account, and thus an extra electrical boundary condition at the liquid-dielectric surface is needed. Therefore the present work aims at generalizing the electrical boundary condition for the ICEK phenomena at liquid-solid interfaces. Theoretically, such derived electric boundary condition presented in this study can be applicable within the entire range of dielectric constant; namely the dielectric constant of materials spans from zero to infinity. It will be demonstrated that the insulating electrical boundary condition for classical fixed-charged electrokinetics and the perfectly conducting electrical boundary condition used in aforementioned studies on ICEK phenomena can be considered as two limiting cases of the present general formulation. Furthermore, with aid of the proposed electrical boundary condition, the ICEO flows over two symmetric polarizable dielectric blocks embedded in the walls of a microchannel driven by a dc electric field will be analyzed. The ICEO flow field will be obtained analytically by solving a biharmonic that governs the stream function to satisfy the Stokes equation. Finally, the effects of the dielectric constant of the polarizable dielectric block and the natural zeta potential of the insulating channel walls on such ICEO flow will be examined.

II. INDUCED ZETA POTENTIAL ON A POLARIZABLE SURFACE OF DIELECTRIC BLOCKS

A. General electrical boundary condition on a polarizable dielectric-liquid interface

To illustrate the process of generating the induced charges at a liquid-dielectric surface in ICEK phenomena, we can envisage a simple case: a dielectric object of arbitrary shape with a polarizable surface immersed in an aqueous solution as shown in Fig. 1(a). When an electric field is applied over the object, the object surface is polarized with acuminated negative charges facing toward the anode of the electric field and an equal amount of positive charges facing toward the cathode of the electric field. Such induced charges on the solid side of the polarizable object surface interact with the ions of the solution to form a screening cloud (i.e., EDL) adjacent to the surface, which in turn causes the electric field lines to be expelled and the ionic flux into the charge cloud to be reduced. At the steady state, once the dipolar induced double layer is formed, the externally applied field exerts a body force on the ions in the screening cloud in the liquid, driving the ions and thus the liquid into motion [see Fig. 1(b)]. It should be pointed out here that the following derivations are based on two assumptions [5]: (i) the surface conduction is negligible compared to the bulk conduction of the electrolyte. This is true for the cases of small Dukhin numbers where the EDL is thin and no electrochemical reaction occurs at the dielectric-liquid interface. (ii) The induced zeta potential is small so that the Debye-Hückel linear ap-

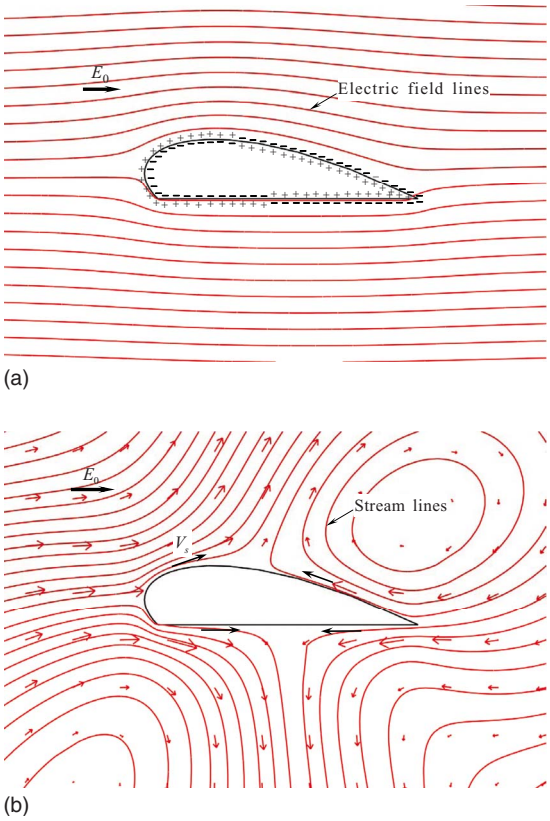

FIG. 1. (Color online) Schematic diagram illustrating the mechanisms of the ICEO. (a) Steady-state electric field distributions around a polarizable dielectric object immersed in an electrolyte solution, where the charge distributions on the surface of the object are due to the polarization of the dielectric block, and the charges inside the EDL are due to the corresponding Coulombic interactions. (b) Steady-state stream lines of ICEO flow driven by the Smoluchowski velocities (V_s) on the surfaced of the polarizable dielectric block.

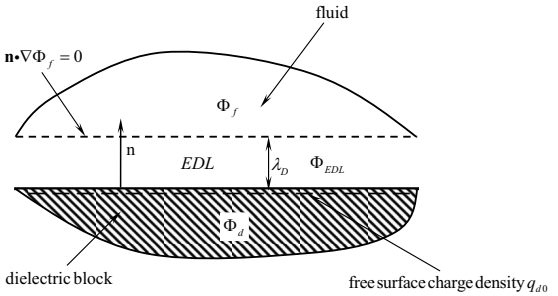

FIG. 2. Schematic diagram for the electric boundary condition for the induced-charge electrokinetic phenomena at the interface between an electrolyte solution and a polarizable dielectric object.

proximation is applicable. With these assumptions, Fig. 1(a) illustrates that under the steady state, the polarizable object behaves like an insulator because an induced dipolar double layer around the polarizable surface is formed and the normal component of electric field does not inject ions into the EDL anymore. This steady-state electrostatic configuration is equivalent to the no-flux electrostatic boundary condition assumed in conventional electrokinetic analysis. In the absence of electrical conductivity gradient in the bulk, the externally applied electric potential outside the EDL at this steady state is governed by Laplace's equation, which is expressed as

$$\nabla^2\Phi_f = 0, \tag{1}$$

with an insulating boundary condition specified at the outer edge of the EDL (the detailed boundary structure is shown in Fig. 2),

$$\mathbf{n}\cdot\nabla\Phi_f|_{n=\lambda_D} = 0, \tag{2}$$

where $\mathbf{n}$ represents a unit vector along n axis (i.e., perpendicular to the polarizable dielectric surface), and λ_D is the Debye screening length that is related to properties of a symmetric electrolyte $(z:z)$ solution through in

$$\lambda_D = \sqrt{\frac{\varepsilon_0\varepsilon_f k_B T}{2n_0 e^2 z^2}},$$

where e is the fundamental charge, z is the valence of the electrolyte ions, n_0 is the bulk number concentration of the electrolyte, k_B is the Boltzmann constant, and T is the absolute temperature of the electrolyte solution. This Debye screening length is normally referred to as the EDL thickness [18]. The EDL is typically nanometers in size, which is why the thin EDL assumptions is usually invoked (and in most cases justified) in microfluidics.

Following Squires and Bazant [19], we also define the induced zeta potential as the potential difference between the potential of fluid at the outer edge of the EDL and the potential on the polarizable dielectric surface. Recall that the potential in the fluid domain is governed by Eqs. (1) and (2). The potential inside the polarizable dielectric body is also governed by Laplace's equation,

$$\nabla^2\Phi_d = 0. \tag{3}$$

It is noted that before the external electric field is imposed, there already exists natural surface charges of density q_{d0} on the dielectric surface. Then the normal component of the electric displacement across the dielectric surface is not continuous, instead with a step jump by amount of q_{d0} [20],

$$\varepsilon_0\varepsilon_f\mathbf{n}\cdot\nabla\Phi_{\mathrm{EDL}}|_{n=0} - \varepsilon_0\varepsilon_d\mathbf{n}\cdot\nabla\Phi_d|_{n=0} = -q_{d0}, \tag{4}$$

where ε_0 is the permittivity of vacuum and has a value of 8.854×10^{-12} F/m, and ε_f and ε_d are, respectively, the dielectric constants of the liquid and the dielectric block. Φ_{EDL} represents the potential inside the EDL, and it matches the bulk potential Φ_f at the outer edge of the EDL through $\Phi_{\mathrm{EDL}}|_{n=\lambda_D} = \Phi_f|_{n=\lambda_D}$ and $\mathbf{n}\cdot\nabla\Phi_{\mathrm{EDL}}|_{n=\lambda_D} = \mathbf{n}\cdot\nabla\Phi_f|_{n=\lambda_D}$. Inside the EDL, the potential is governed by Poisson's equation,

$$\nabla^2\Phi_{\mathrm{EDL}} = -\frac{\rho_e}{\varepsilon_0\varepsilon_f}, \tag{5}$$

where ρ_e is the net charge density inside the EDL. Then with an assumption of thin EDL, the EDL can be approximated as a local planer geometry as shown in Fig. 2, and hence Eq. (5) is reduced to

$$\varepsilon_0\varepsilon_f\frac{\partial^2\Phi_{\mathrm{EDL}}}{\partial n^2} = -\rho_e. \tag{6}$$

Integrating Eq. (6) from the polarizable dielectric surface to the outer edge of the EDL, we can write

$$\varepsilon_0\varepsilon_f\int_0^{\lambda_D}\frac{\partial^2\Phi_{\mathrm{EDL}}}{\partial n^2}dn = -\int_0^{\lambda_D}\rho_e dn. \tag{7}$$

Note that the upper limit of the integration, $n=\lambda_D$ physically represents the outer edge of the EDL. The right-hand side of Eq. (7) gives the total amount of charges stored in the EDL capacitor, which can be related to the potential drop across the EDL, $\Phi_f|_{n=\lambda_D} - \Phi_d|_{n=0}$, the thickness of the EDL, λ_D, and the electric permittivity of the fluid, $\varepsilon_0\varepsilon_f$. For the left-hand side of Eq. (7), it is easy to show that $\partial\Phi_{\mathrm{EDL}}/\partial n$ vanishes at the outer edge of the EDL. Hence, based on Eq. (7), the electric displacement at the fluid-solid interface on the fluid side can be approximated as

$$\varepsilon_0\varepsilon_f\mathbf{n}\cdot\nabla\Phi_{\mathrm{EDL}}|_{n=0} = \varepsilon_0\varepsilon_f\frac{\Phi_f|_{n=\lambda_D} - \Phi_d|_{n=0}}{\lambda_D} \tag{8}$$

which represents the amount of charges (including both natural and induced parts) stored in the EDL capacitor near a polarizable dielectric surface when the potential drop across the EDL is small [21]. These charges induce same amount of opposite surface charges on the dielectric block, which are responsible for the ICEK phenomena.

Utilizing Eqs. (4) and (8), we can obtain a boundary condition of Robin type for the potential distribution inside the polarizable dielectric object,

$$\Phi_d|_{n=0} + \lambda_D\frac{\varepsilon_d}{\varepsilon_f}\mathbf{n}\cdot\nabla\Phi_d|_{n=0} = \Phi_f|_{n=\lambda_D} + \zeta_{d0}, \tag{9}$$

where ζ_{d0} is the zeta potential corresponding to natural surface charges q_{d0}, and is related to q_{d0} by [5]

$$\zeta_{d0} = \frac{\lambda_D q_{d0}}{\varepsilon_0 \varepsilon_f}. \tag{10}$$

Through the boundary condition (9), the potential inside the polarizable dielectric object and the potential in the bulk fluid domain (namely outside the EDL) are coupled together, and thus the potential inside the dielectric object can be obtained by solving Eq. (3) since the electrical potential distribution in the bulk fluid domain has already been determined by Eqs. (1) and (2). Finally, the total zeta potential can be found as the difference between the potential at the outer edge of the EDL and the potential on the dielectric object surface, and it takes the following form [19]:

$$\zeta_d = \Phi_d|_{n=0} - \Phi_f|_{n=\lambda_D} = -\lambda_D \frac{\varepsilon_d}{\varepsilon_f} \mathbf{n} \cdot \nabla \Phi_d|_{n=0} + \zeta_{d0}. \tag{11}$$

Besides the conventional zeta potential ζ_{d0} due to natural charges on the dielectric surface, it is revealed by Eq. (11) that an extra zeta potential $\zeta_{di} = -\lambda_D \varepsilon_d \mathbf{n} \cdot \nabla \Phi_d|_{n=0} / \varepsilon_f$ is induced due to the presence of external electric field. Obviously, the induced zeta potential ζ_{di} is no longer a constant, instead it varies with local electric field strength at the polarizable dielectric object surface.

The proposed electric boundary condition shown in Eq. (11) is general because two important limiting cases can be obtained from it. For the case of insulating surfaces (i.e., $\varepsilon_d \to 0$), the electric boundary condition for conventional electrokinetic flows can be recovered when the induced part of the zeta potential ζ_{di} drops off and only the natural zeta potential ζ_{d0} remains. On the other hand, when an object has excellent electric conductibility (i.e., $\varepsilon_d \to \infty$), a perfect conductor should have equipotential, that is, $\Phi_d = \zeta_{d0}$. Utilizing Eq. (9), we can show that the induced zeta potential is just the opposite potential outside the edge of the EDL layer in the liquid domain, i.e., $-\Phi_f|_{n=\lambda_D}$; this is consistent with Squires and Bazant's analysis for perfectly polarizable surfaces (i.e., $\varepsilon_d \to \infty$) [5].

B. Induced zeta potential on the surface of two polarizable dielectric blocks embedded in the wall of a slit microchannel

Consider an electrolyte solution in a parallel-plate slit channel of height $2H$ as shown in Fig. 3. Two symmetric polarizable dielectric blocks are embedded in the microchannel walls, and they have an arbitrary dielectric constant ε_d and geometric dimensions of $aH \times bH$ (where a and b, respectively, are length and height scale factors of the polarizable dielectric block with respect to the half height H of the channel). Once in contact with electrolyte solution, the polarizable dielectric surface is charged with a uniform natural zeta potential ζ_{d0}. The rest of the channel wall is electrically insulating and also has a uniform natural zeta potential ζ_0. With the thin EDL approximation, the electric field in the fluid domain is one dimensional, i.e., $\mathbf{E} = E_0 \mathbf{e}_x$, which gives a linear profile of the applied electrical potential in the bulk fluid domain, $\Phi_f = -E_0 x + C$ (here C is a constant). Due to symmetry, analyses of both the electric problem and the flow problem in the next section are restricted in the lower half of

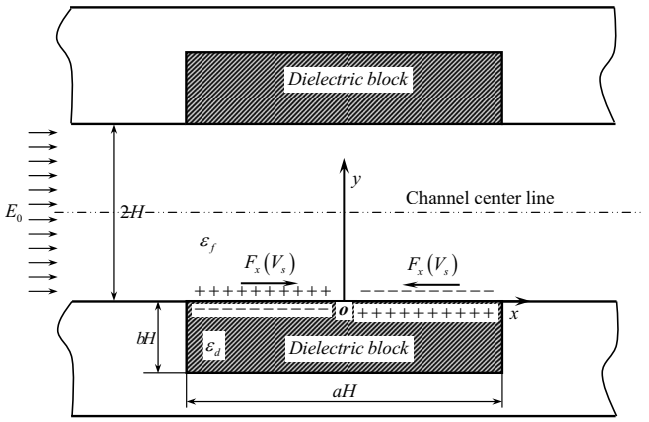

FIG. 3. Schematic of two symmetric polarizable dielectric blocks embedded in the walls of an infinitely long insulating slit microchannel. After application of an external electric field E_0, the dielectric block is polarized so that the left-hand side of the object's surface acquires negative surface charges and the right-hand side of its surface acquires positive surface charges. In order to maintain the electrical neutrality in the entire system, the net charge density in the EDL near the left-hand side of the surface should be positive ($\rho_e > 0$) and the net charge density in the EDL near the right-hand side of the surface should be negative ($\rho_e < 0$). Obviously, the interaction of the external electric field and these two charge densities generates two electric body forces F_x ($=\rho_e E_0$) (with opposite directions inside the EDL), thereby resulting in two Smoluchowski slip velocities V_s (with opposite directions), which are responsible for the flow patterns generated above the dielectric block surface.

the channel domain. Hence, to determine the induced zeta potential on the dielectric surface, we need to know the electrical potential distributions inside the dielectric block. Since there is no free charge inside the dielectric block, the electric potential in the dielectric block domain is governed by Laplace's equation

$$\nabla^2 \Phi_d = 0. \tag{12}$$

The appropriate boundary conditions are specified as

$$\Phi_d|_{y=0} + \frac{\varepsilon_d}{\varepsilon_f} \lambda_D \left. \frac{\partial \Phi_d}{\partial y} \right|_{y=0} = -E_0 x + \zeta_{d0}, \tag{13a}$$

$$\left. \frac{\partial \Phi_d}{\partial y} \right|_{y=-bH} = 0 \qquad \left. \frac{\partial \Phi_d}{\partial x} \right|_{x=-aH/2} = 0 \qquad \left. \frac{\partial \Phi_d}{\partial x} \right|_{x=aH/2} = 0. \tag{13b}$$

Defining the following nondimensional groups:

$$\bar{\Phi}_d = \frac{\Phi_d}{E_0 H} \quad \bar{\zeta}_{d0} = \frac{\zeta_{d0}}{E_0 H} \quad \bar{x} = \frac{x}{H} \quad \bar{y} = \frac{y}{H}, \tag{14}$$

we can nondimensionalize Eq. (12), which is expressed in the Cartesian coordinate as

$$\frac{\partial^2 \bar{\Phi}_d}{\partial \bar{x}^2} + \frac{\partial^2 \bar{\Phi}_d}{\partial \bar{y}^2} = 0. \tag{15}$$

The dimensionless boundary conditions can be rewritten as

$$\bar{\Phi}_d|_{\bar{y}=0} + \frac{\varepsilon_d}{\varepsilon_f}\frac{\lambda_D}{H}\left.\frac{\partial\bar{\Phi}_d}{\partial\bar{y}}\right|_{\bar{y}=0} = -\bar{x} + \bar{\zeta}_{d0}, \tag{16a}$$

$$\left.\frac{\partial\bar{\Phi}_d}{\partial\bar{y}}\right|_{\bar{y}=-b} = 0 \qquad \left.\frac{\partial\bar{\Phi}_d}{\partial\bar{x}}\right|_{\bar{x}=-a/2} = 0 \qquad \left.\frac{\partial\bar{\Phi}_d}{\partial\bar{x}}\right|_{\bar{x}=a/2} = 0. \tag{16b}$$

Without otherwise specification, the other potentials and geometric dimensions are also scaled by E_0H and H, respectively. Using the separation of variables method, we can show that the electric potential inside the polarizable dielectric block takes the form

$$\bar{\Phi}_d(\bar{x},\bar{y}) = \bar{\zeta}_{d0} + \sum_{n=1}^{\infty}(A_n e^{\mu_n\bar{y}} + B_n e^{-\mu_n\bar{y}})\cos\left[\mu_n\left(\bar{x}+\frac{a}{2}\right)\right], \tag{17}$$

where the coefficient A_n and B_n are given by

$$A_n = \frac{2[1-(-1)^n]}{a\mu_n^2}\frac{e^{2\mu_n b}}{(1-\beta\mu_n)+(1+\beta\mu_n)e^{2\mu_n b}}, \tag{18a}$$

$$B_n = \frac{2[1-(-1)^n]}{a\mu_n^2}\frac{1}{(1-\beta\mu_n)+(1+\beta\mu_n)e^{2\mu_n b}}. \tag{18b}$$

Here β is a dimensionless parameter defined as [22]

$$\beta = \frac{\varepsilon_d/\varepsilon_f}{H/\lambda_D}, \tag{19}$$

which physically characterizes the relative importance of the associated electrical properties $(\varepsilon_d/\varepsilon_f)$ and the electrokinetic channel size (H/λ_D). The dimensionless parameter β may also be viewed as a ratio of capacitances: namely, the ratio of the block capacitance ε_d/H to the double-layer capacitance ε_f/λ_D. The physical interpretation is that for an ideally polarizable dielectric $\beta\to\infty$ (i.e., a conductor with infinite capacitance) there is zero potential dropped over the dielectric and hence all potential is dropped over the double layer, giving the maximal induced zeta potential and thus ICEK phenomena. For a dielectric with finite ε_d, then β is finite and hence some potential is dropped across the dielectric, thereby reducing the induced zeta potential and hence ICEK phenomena. The eigenvalues μ_n are determined from

$$\mu_n = \frac{n\pi}{a} \quad n = 1,2,3\ldots \tag{20}$$

As mentioned early, the total zeta potential $\bar{\zeta}_d$ on a polarizable dielectric surface can be found as the difference between the potential on the polarizable dielectric surface and the potential at the outer edge of the EDL. Furthermore, the total zeta potential can be decomposed into two parts: (i) $\bar{\zeta}_{d0}$ due to the natural surface charges and (ii) $\bar{\zeta}_{di}$ due to the induced charges, and thus is given by

$$\bar{\zeta}_d = \bar{\Phi}_d|_{\bar{y}=0} - \bar{\Phi}_f|_{\bar{y}=\lambda_D/H} = \bar{\zeta}_{d0} + \bar{\zeta}_{di}, \tag{21}$$

where $\bar{\zeta}_{di}$ can be determined with aid of Eq. (17) as

$$\bar{\zeta}_{di} = -\left.\beta\frac{\partial\bar{\Phi}_d}{\partial\bar{y}}\right|_{\bar{y}=0} = -\beta\sum_{n=1}^{\infty}\mu_n(A_n - B_n)\cos\left[\mu_n\left(\bar{x}+\frac{a}{2}\right)\right]. \tag{22}$$

For completely insulating blocks (i.e., $\beta=0$), it can be readily shown from Eq. (22) that the induced zeta potential $\bar{\zeta}_{di}$ is zero, and thus the zeta potential on the electrically insulating block surface contains $\bar{\zeta}_{d0}$ only. This is the case for the classical linear electrokinetic phenomena with natural fixed charges. On the other hand, for perfectly conducting (or polarizable) blocks (i.e., $\beta\to\infty$), it also can be shown that Eq. (22) can be simplified to

$$\bar{\zeta}_{di} = \sum_{n=1}^{\infty}\frac{2[(-1)^n-1]}{a\mu_n^2}\cos\left[\mu_n\left(\bar{x}+\frac{a}{2}\right)\right]. \tag{23}$$

Note that the right-hand side of Eq. (23) in fact is the Fourier series expansion of the function $\bar{x}$. Hence, we can obtain $\bar{\zeta}_{di}=\bar{x}=-\bar{\Phi}_f$. This result is exactly the same as the analytical result of Squires and Bazant [5] for perfectly polarizable surfaces.

III. FLOW FIELD OF ICEO IN A SLIT MICROCHANNEL EMBEDDED WITH TWO POLARIZABLE DIELECTRIC BLOCKS

With a dc electric field, E_0 applied along the axial direction of an infinitely long slit microchannel as shown in Fig. 3, the electrolyte in the microchannel experiences an electrostatic body force $\rho_e E_0$ (i.e., Lorentz force), where ρ_e is the net charge density due to the EDL of the channel. However, as this electrostatic body force is present only within the EDL which is very thin compared to the channel depth, the flow can be considered as triggered by a moving boundary wall. Therefore, the fully developed flow field for low Reynolds number creeping flows (i.e., $\mathrm{Re}\ll 1$) of an incompressible Newtonian fluid is two dimensional and is governed by the continuity equation and the Stokes equation [23],

$$\nabla\cdot\mathbf{V} = 0, \tag{24a}$$

$$-\nabla p + \mu\nabla^2\mathbf{V} = 0, \tag{24b}$$

with an implicit slip boundary condition given by the Helmholtz-Smoluchowski equation

$$\mathbf{V} = -\frac{\varepsilon_0\varepsilon_f\zeta}{\mu}\mathbf{E} \tag{25}$$

where $\mathbf{V}$ is the velocity vector expressed as $\mathbf{V}=u\mathbf{e}_x+v\mathbf{e}_y$, $\mathbf{E}$ is the electric field strength vector and it can be expressed as $\mathbf{E}=E_0\mathbf{e}_x$, p is the hydrodynamic pressure, ζ is the zeta potential of the channel wall, and μ is the dynamic viscosity of the electrolyte solution. As shown in Fig. 3, along the channel wall the zeta potential can be modeled by three segments: (i) when $x<-aH/2$ and (ii) when $x>aH/2$, the wall is completely electrically insulating, and has a uniform natural zeta potential of ζ_0. (iii) When $-aH/2\le x\le aH/2$, the channel wall is polarizable dielectric surface. Besides the conven-

tional zeta potential ζ_{d0}, there is an extra induced zeta potential ζ_{di} under applied external electric field. It is evident that the zeta potential exhibits step change at two conjunction points: $x=-aH/2$ and $x=aH/2$, which will result in a jump in the Helmholtz-Smoluchowski slip velocity along the microchannel according to Eq. (25).

It can be readily shown that the governing equation Eqs. (24) can be transformed into a biharmonic equation in terms of the stream function [23]

$$\nabla^4\Psi = 0, \tag{26}$$

which can be further expressed in Cartesian coordinates as

$$\frac{\partial^4\Psi}{\partial x^4} + 2\frac{\partial^4\Psi}{\partial x^2 y^2} + \frac{\partial^4\Psi}{\partial y^4} = 0. \tag{27}$$

The two velocity components can be expressed as two spatial derivatives of the stream function

$$u = \frac{\partial\Psi}{\partial y} \quad v = -\frac{\partial\Psi}{\partial x}. \tag{28}$$

Assuming that the flow far away from the polarizable dielectric patch is undisturbed, the magnitude of the velocity is given by the Helmholtz-Smoluchowski velocity expressed by

$$V_\infty = -\frac{\varepsilon_0\varepsilon_f\zeta_0 E_0}{\mu}. \tag{29}$$

With aid of Eqs. (28) and (29), the proper boundary conditions can be prescribed for the stream function as

$$\left.\frac{\partial\Psi}{\partial x}\right|_{y=0} = 0 \quad |x| < \infty, \tag{30a}$$

$$\left.\frac{\partial\Psi}{\partial y}\right|_{y=0} = \begin{cases} -\dfrac{\varepsilon_0\varepsilon_f\zeta_0 E_0}{\mu}, & x < -\dfrac{aH}{2} \text{ and } x > \dfrac{aH}{2} \\ -\dfrac{\varepsilon_0\varepsilon_f\zeta_d E_0}{\mu}, & -\dfrac{aH}{2} \le x \le \dfrac{aH}{2}, \end{cases} \tag{30b}$$

$$\left.\frac{\partial\Psi}{\partial x}\right|_{y=H} = 0 \quad \left.\frac{\partial^2\Psi}{\partial y^2}\right|_{y=H} = 0 \quad |x| < \infty, \tag{30c}$$

$$\Psi \to V_\infty y \quad \text{as} \quad |x| \to \infty, \tag{30d}$$

where ζ_d denotes the dimensional total zeta potential on the polarizable dielectric surface and its dimensionless counterpart is $\bar{\zeta}_d$.

Because of linearity, we can decompose the total stream function as

$$\Psi = \Psi_\infty + \Psi_d, \tag{31}$$

where $\Psi_\infty = V_\infty y$, which is the stream function for the far away flow field. Ψ_d is the stream function due to the disturbance of the polarizable dielectric patch and it also satisfies the biharmonic equation.

Nondimensionalizing all stream functions (Ψ, Ψ_∞, and Ψ_d) with respect to $V_\infty H$, we can write the governing equation for the induced stream function Ψ_d in dimensionless form $\bar{\Psi}_d$ as

$$\frac{\partial^4\bar{\Psi}_d}{\partial\bar{x}^4} + 2\frac{\partial^4\bar{\Psi}_d}{\partial\bar{x}^2\bar{y}^2} + \frac{\partial^4\bar{\Psi}_d}{\partial\bar{y}^4} = 0. \tag{32}$$

The corresponding boundary conditions can be formulated as

$$\left.\frac{\partial\bar{\Psi}_d}{\partial\bar{x}}\right|_{\bar{y}=0} = 0 \quad |\bar{x}| < \infty, \tag{33a}$$

$$\left.\frac{\partial\bar{\Psi}_d}{\partial\bar{y}}\right|_{\bar{y}=0} = \begin{cases} 0, & \bar{x} < -\dfrac{a}{2} \text{ and } \bar{x} > \dfrac{a}{2} \\ \dfrac{\bar{\zeta}_d}{\bar{\zeta}_0} - 1, & -\dfrac{a}{2} \le x \le \dfrac{a}{2}, \end{cases} \tag{33b}$$

$$\left.\frac{\partial\bar{\Psi}_d}{\partial\bar{x}}\right|_{\bar{y}=1} = 0 \quad \left.\frac{\partial^2\bar{\Psi}_d}{\partial\bar{y}^2}\right|_{\bar{y}=1} = 0 \quad |x| < \infty, \tag{33c}$$

$$\bar{\Psi}_d \to 0 \quad \text{as} \quad |\bar{x}| \to \infty. \tag{33d}$$

Furthermore, with the Fourier transform [24]

$$\bar{\Psi}_d^k(k,\bar{y}) = \frac{1}{\sqrt{2\pi}}\int_{-\infty}^{+\infty}\bar{\Psi}_d(\bar{x},\bar{y})e^{-ik\bar{x}}d\bar{x}, \tag{34}$$

the biharmonic Eq. (32) can be converted into a fourth-order ordinary differential equation,

$$\frac{d^4\bar{\Psi}_d^k}{d\bar{y}^4} - 2k^2\frac{d^2\bar{\Psi}_d^k}{d\bar{y}^2} + k^4\bar{\Psi}_d^k = 0. \tag{35}$$

The boundary conditions are also transformed into the Fourier domain accordingly, and they become

$$\bar{\Psi}_d^k|_{\bar{y}=0} = 0 \quad \left.\frac{d\bar{\Psi}_d^k}{d\bar{y}}\right|_{\bar{y}=0} = Z(k), \tag{36a}$$

$$\bar{\Psi}_d^k|_{\bar{y}=1} = 0 \quad \left.\frac{d^2\bar{\Psi}_d^k}{d\bar{y}^2}\right|_{\bar{y}=1} = 0, \tag{36b}$$

where the auxiliary function $Z(k)$ is defined by

$$Z(k) = \frac{1}{\sqrt{2\pi}}\int_{-\frac{a}{2}}^{+\frac{a}{2}}\left(\frac{\bar{\zeta}_d}{\bar{\zeta}_0} - 1\right)e^{-ik\bar{x}}dx. \tag{37}$$

Then, substitution of Eqs. (21) and (22) into Eq. (37) gives an explicit expression for $Z(k)$,

$$Z(k) = -\frac{1}{\sqrt{2\pi}}\frac{\beta}{\bar{\zeta}_0}\sum_{n=1}^{\infty}\mu_n(A_n - B_n)\frac{ik[-e^{iak/2} + (-1)^n e^{-iak/2}]}{k^2 - \mu_n^2} + \frac{1}{\sqrt{2\pi}}\frac{\bar{\zeta}_{d0} - \bar{\zeta}_0}{\bar{\zeta}_0}\frac{2\sin\left(\dfrac{ak}{2}\right)}{k}. \tag{38}$$

The solution of the stream function in the k domain is

$$\bar{\Psi}_d^k(k,\bar{y}) = C_1(k)\sinh(k\bar{y}) + C_2(k)\bar{y}\cosh[k(\bar{y}-1)], \quad (39)$$

where two coefficients are determined by

$$C_1(k) = \frac{-2}{\sinh(2k)-2k}Z(k), \quad (40a)$$

$$C_2(k) = \frac{2\sinh(k)}{\sinh(2k)-2k}Z(k). \quad (40b)$$

Finally, the induced stream function can be obtained by using the inverse Fourier transform

$$\bar{\Psi}_d(\bar{x},\bar{y}) = \frac{1}{\sqrt{2\pi}}\int_{-\infty}^{+\infty}\bar{\Psi}_d^k(k,\bar{y})e^{ik\bar{x}}dk \quad (41)$$

and the total stream function is constructed through Eq. (31),

$$\bar{\Psi}(\bar{x},\bar{y}) = \bar{y} + \frac{1}{\sqrt{2\pi}}\int_{-\infty}^{+\infty}\bar{\Psi}_d^k(k,\bar{y})e^{ik\bar{x}}dk. \quad (42)$$

Likewise, the dimensionless velocity field is obtained by substituting Eq. (42) into Eq. (28),

$$\bar{u}(\bar{x},\bar{y}) = 1 + \frac{1}{\sqrt{2\pi}}\int_{-\infty}^{+\infty}\frac{d\bar{\Psi}_d^k(k,\bar{y})}{dy}e^{ik\bar{x}}dk, \quad (43a)$$

$$\bar{v}(\bar{x},\bar{y}) = -\frac{1}{\sqrt{2\pi}}\int_{-\infty}^{+\infty}(ik)\bar{\Psi}_d^k(k,\bar{y})e^{ik\bar{x}}dk, \quad (43b)$$

where $\bar{u}=u/V_\infty$ and $\bar{v}=v/V_\infty$.

The remaining task is to evaluate the integrations with respect to k. To obtain analytical solutions for the integrations in Eqs. (42) and (43), the residue theorem [25] is invoked, where the infinite integral of an function can be converted to an summation of residues at all singularity points of this function. Then we can, respectively, show that the solutions for the dimensionless stream function, the horizontal velocity component, and the vertical velocity component are

$$\bar{\Psi}(\bar{x},\bar{y}) = \bar{y} + (-1)^c\sqrt{2\pi}i\sum_{m=1}^{\infty}\frac{Z(k_m)e^{ik_m\bar{x}}}{\cosh(2k_m)-1} \times\{-\sinh(k_m\bar{y}) + \sinh(k_m)\bar{y}\cosh[k_m(\bar{y}-1)]\}, \quad (44a)$$

$$\bar{u}(\bar{x},\bar{y}) = 1 + (-1)^c\sqrt{2\pi}i\sum_{m=1}^{\infty}\frac{Z(k_m)e^{ik_m\bar{x}}}{\cosh(2k_m)-1} \times\{-\cosh(k_m\bar{y})k_m + \sinh(k_m)\cosh[k_m(\bar{y}-1)] + k_m\sinh(k_m)\bar{y}\sinh[k_m(\bar{y}-1)]\}, \quad (44b)$$

$$\bar{v}(\bar{x},\bar{y}) = (-1)^c\sqrt{2\pi}\sum_{m=1}^{\infty}\frac{Z(k_m)k_m e^{ik_m\bar{x}}}{\cosh(2k_m)-1} \times\{-\sinh(k_m\bar{y}) + \sinh(k_m)\bar{y}\cosh[k_m(\bar{y}-1)]\}, \quad (44c)$$

where k_m is the complex root of the eigenfunction $\sinh(2k_m)-2k_m=0$. When $\bar{x}>0$, $c=0$ and the summation is taken for all k_m with positive imaginary part; when $\bar{x}<0$, $c=1$ and the summation is carried out for all k_m with negative imaginary part. Table I provides the first five complex roots of the above eigenfunction computed using MATHEMATICA 6.0 with high accuracy of 10^{-10}. Moreover, as $\bar{x}\to 0$ from both domains (i.e., $\bar{x}>0$ and $\bar{x}<0$), we can check that an identical value is obtained, which ensures that the present analytical solutions are continuous at $\bar{x}=0$.

TABLE I. First five eigenvalues determined form the eigenfunction, $\sinh(2k_m)-2k_m=0$. Note: the complex conjugates of k_m are another half of eigenvalues. Eigenvalues determined form the eigenfunction, $\sinh(2k_m)-2k_m=0$.

m	k_m
1	±1.3843391414+3.7488381388i
2	±1.6761049424+6.9499798569i
3	±1.8583838398+10.1192588539i
4	±1.9915708201+13.2772736327i
5	±2.0966257352+16.4298705025i

IV. RESULTS AND DISCUSSION

In this section, a special case study is presented to show the basic flow patterns of ICEO flow above the polarizable block embedded in the channel wall. Then by using the analytical solutions, parametric studies are carried out to examine the effects of the dielectric constant of the polarizable dielectric block and the natural zeta potential of the electrically insulting part of the channel wall on flow patterns of ICEO flows In all calculations, the polarizable dielectric blocks are assumed to have fixed dimensionless dimensions of $a=5$ and $b=5$. Moreover, since the focus of this study is placed on the induced-charge effects, the effect of the natural surface charges on the polarizable dielectric block surface is excluded by assuming $\bar{\zeta}_{d0}=0$.

A. Basic flow patterns of ICEO flows

Since to our best knowledge, no other analytical solutions of ICEO flows are available in this geometry in the literature, a specific case study is conducted to present the basic flow patterns of ICEO flows above the polarizable dielectric block. In this special case, we consider a limiting case of $\beta\to\infty$ when the polarizable dielectric block is a perfect conductor and thus has greatest polarizability. The dimensionless natural zeta potential on both upstream and downstream of the insulating microchannel $\bar{\zeta}_0$ is set as −0.1, which may represent a practical situation where $E_0=100$ V/cm, $H=50$ μm, and $\zeta_0=-50$ mV.

The calculated results are shown in Fig. 4 which includes the horizontal velocity component $\bar{u}$, the vertical velocity comment $\bar{v}$, and the velocity vector field. It is seen that from two figures in Fig. 4(a), the fluid near the channel wall moves to the block center (i.e., $\bar{x}=0$ and $\bar{y}=0$) with large velocity from two sides; however the velocity decreases as

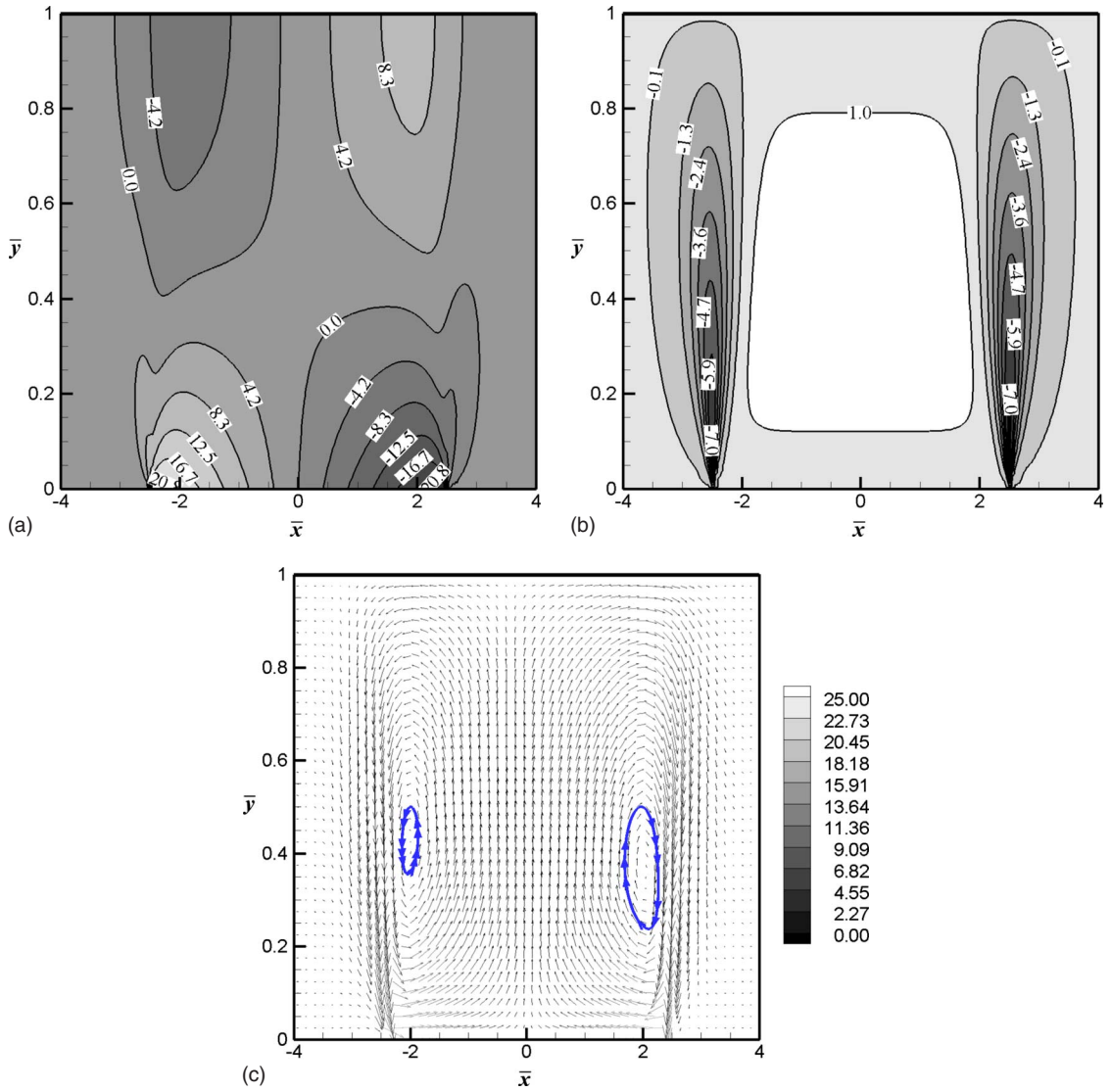

FIG. 4. (Color online) Analytical solutions derived in the present study for (a) horizontal component of velocity $\bar{u}$, (b) vertical component of velocity $\bar{v}$, and (c) velocity vector field. Calculations are conducted for the ICEO flow above a perfectly polarizable ($\beta \to \infty$) block with $a=5$, $b=5$, and the dimensionless natural zeta potential for the perfectly polarizable block $\bar{\zeta}_{d0}=0$, and the insulating wall $\bar{\zeta}_0=-0.1$.

approaching to the block centerline (i.e., $\bar{x}=0$). Near the block centerline, the flow changes its direction with flow moving toward the block centerline near the channel wall region (i.e., $\bar{y}=0$) and flow, leaving away from the block centerline in the channel center line region (i.e., $\bar{y}=1$). As shown in Fig. 3, on the left side of the block surface (i.e., $\bar{x}<0$), the external electric field induces negative surface charges (also negative induced zeta potential); while on the right side of the block (i.e., $\bar{x}>0$), the positive surface charges (also positive induce zeta potential) are induced. Accordingly the resultant slip velocity is positive on the left side and is negative on the right side of the block based on the expression of the Smoluchowski velocity given by Eq. (29). Also, on the block surface, the magnitude of the horizontal velocity component can reach twenty times larger than that of the natural charge driven electro-osmotic flow in upstream and downstream of the insulating channels regions. This is attributed to the fact that the Helmholtz-Smoluchowski slip velocity on conducting surfaces is proportional to E_0^2 [26], while the Smoluchowski slip velocity driven by natural charges is just proportional to E_0. Since the flow rate is determined by the natural charge driven electro-osmotic flow in the regions of insulating channel, in order to fulfill the mass conservation there must be velocity reversal on both sides of the channel centerline (i.e., $\bar{y}=1$). For a sufficiently large natural zeta potential on the insulating wall, the ICEO flow over the polarizable blocks may not dominate the electro-osmotic flow over the insulating walls; i.e., it is only because the natural zeta is not too large that the dominance of ICEO is observed. From the vertical velocity distributions shown in Fig. 4(b), it is noted that the fluid in a large portion around the block centerline region moves upwards to the channel centerline at a velocity comparable to the incoming flow from infinity ($\bar{x} \to \pm\infty$). Above the two edges of the polarizable block, the fluid flows down very fast to the polarizable surface. All these features are resulted from the fact

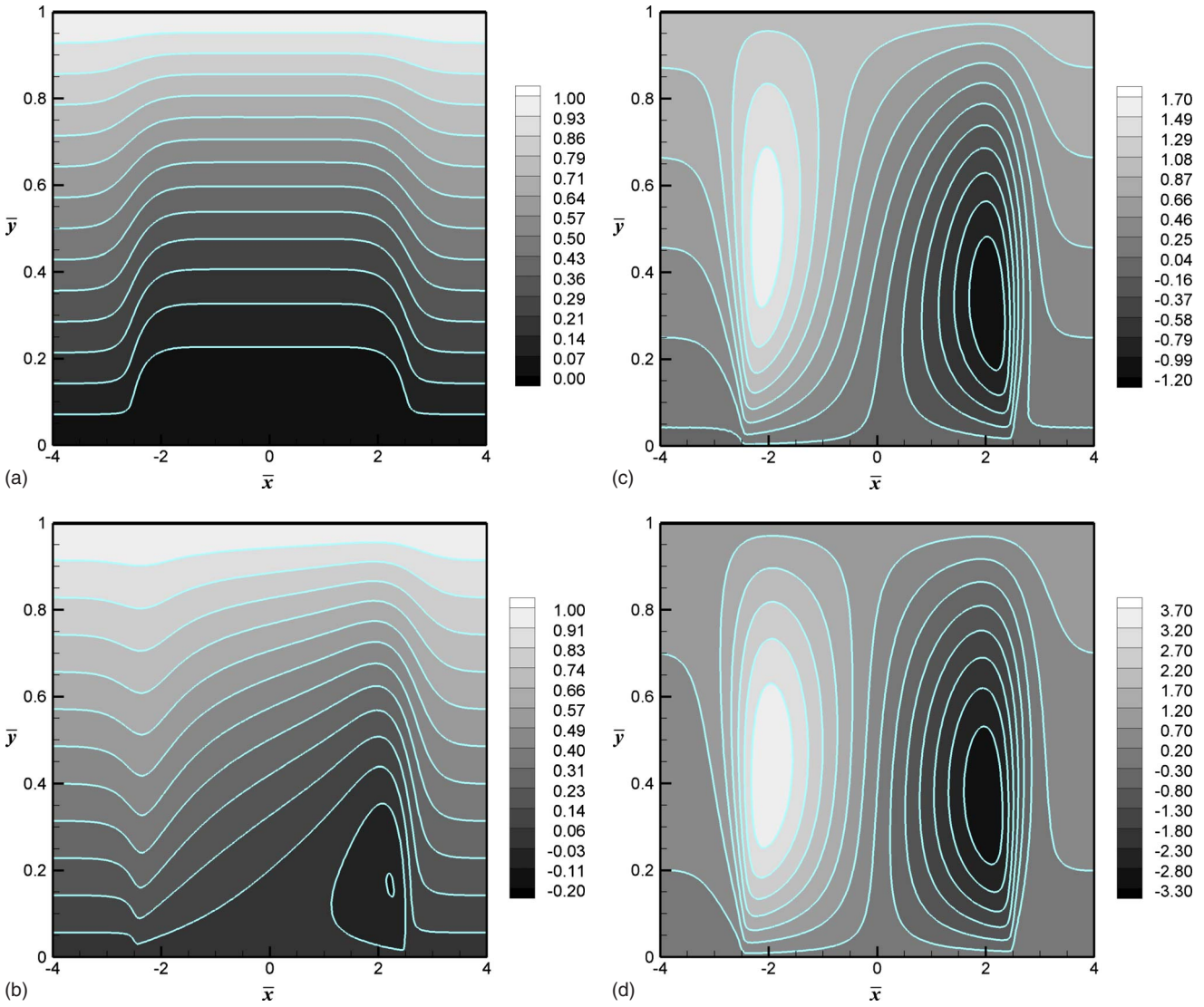

FIG. 5. (Color online) Dimensionless stream function $\bar{\Psi}$ contour above a polarizable dielectric block for four different β values: (a) $\beta=0$, (b) $\beta=0.1$, (c) $\beta=1$, and (d) $\beta\to\infty$. Other parameters in the calculations are $a=5$, $b=5$, the dimensionless natural zeta potential for the polarizable block $\bar{\zeta}_{d0}=0$, and the insulating wall $\bar{\zeta}_0=-0.1$.

that there should be no net flow along y direction. Figure 4(c) shows the analytical solution computed using Eqs. (44), which gives high resolution of the velocity vector field. It is shown that there is a pair of counter-rotating vortices above the polarizable surface. The generation of a vortices pair on a planar polarizable surface was also conceptualized in [27].

B. Parametric study of ICEO flow patterns

Figure 5 shows the effect of β on the flow patterns over the bottom polarizable dielectric block. The normalized stream function has a value of zero on the channel walls and unit one at the channel centerline. The difference of the stream function between two locations in the flow field represents the steady-state volumetric flow rate passing through the cross-section line determined by theses two locations. Since there exists a uniform velocity profile at both upstream and downstream of the channel, the stream function should be linearly proportional to y and the stream lines are exactly in parallel with x axis in the two insulating regions of the channel. Showing in Fig. 5(a) corresponds to the case of $\beta=0$, indicating that the block is not polarizable. Furthermore, with the assumption of no natural surface charges on the block surface, $\zeta_{d0}=0$, no driving force is present for the fluid over the block. Hence, no slip boundary condition on the block surface causes velocity profile to exhibit a parabolic shape and the stream function depends on y^3, which explains the stream line distributions above the dielectric surface shown in Fig. 5(a). As β increases, the dielectric block becomes polarizable. Then, a small clockwise vortex is formed above the right portion of the polarizable dielectric surface as shown in Fig. 5(b). With such magnitude of β, the induced zeta potential on the left portion of the block is of the same order and the same sign as the natural zeta potential on the insulating channel wall. The resultant two Helmholtz-Smoluchowski slip velocities on the left portion of the polar-

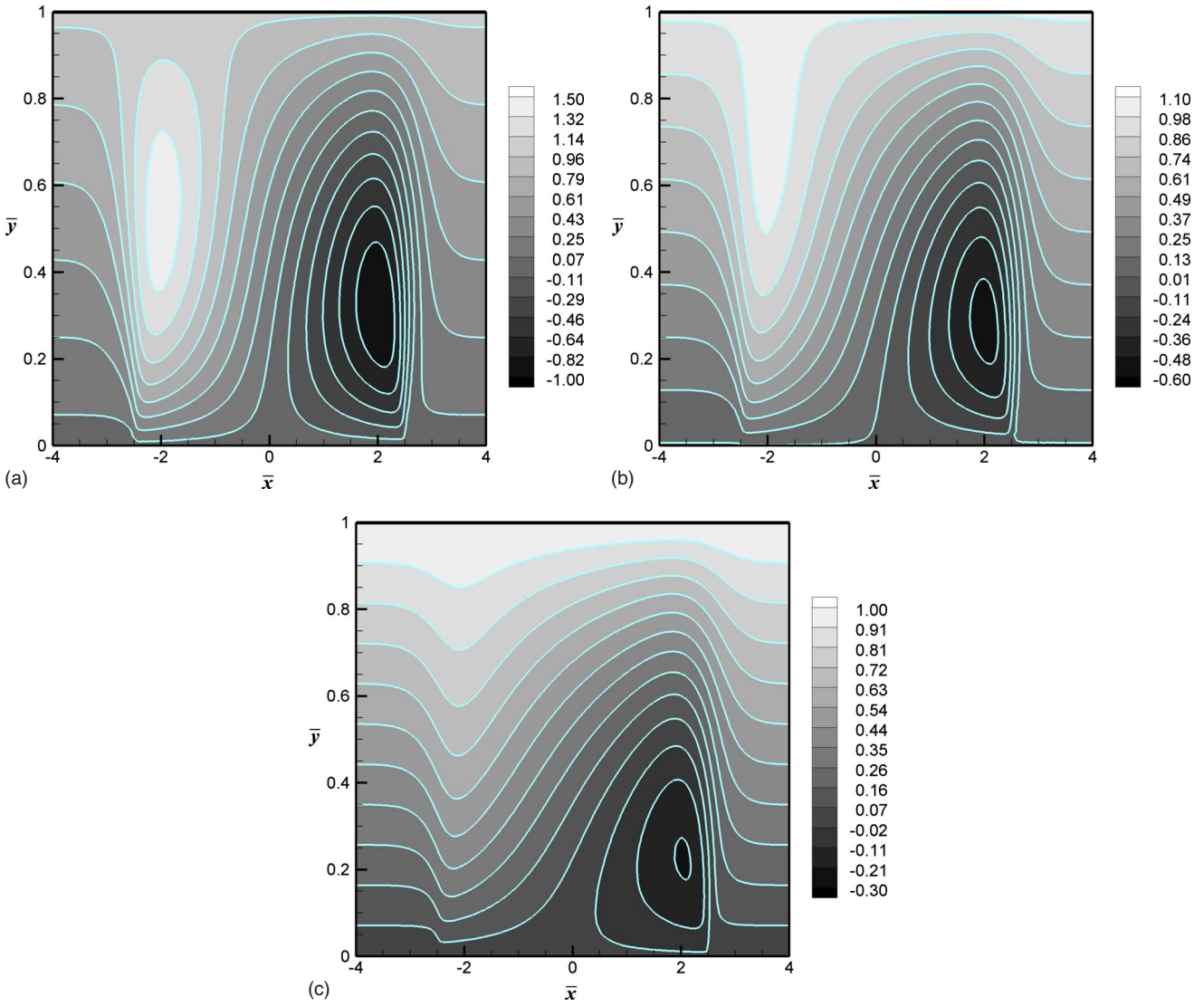

FIG. 6. (Color online) Dimensionless stream function $\bar{\Psi}$ contour above a perfectly polarizable block ($\beta \to \infty$) for three different $\bar{\zeta}_0$ values: (a) $\bar{\zeta}_0 = -0.3$, (b) $\bar{\zeta}_0 = -0.5$, and (c) $\bar{\zeta}_0 = -1.0$. Other parameters in the calculations are $a=5$, $b=5$, and the dimensionless natural zeta potential for the polarizable block $\bar{\zeta}_{d0}=0$.

izable surface and the upstream insulting surfaces are of similar magnitude and also in the same direction. Hence, the flow speeds up near the polarizable dielectric block and slows down near the channel centerline to fulfill the mass conservation of fluid, but no circulating flow is developed on the left portion of the block. However, on the right portion of the polarizable dielectric surface, nonzero value of β always produces a negative slip velocity (in opposite to the main flow stream), thereby giving rise to the development of a vortex. As shown in Fig. 5(c), further increasing β causes the dielectric surface more polarizable to induce a larger zeta potential on the left surface, which in turn produces a larger slip velocity (compared to the slip velocity from the infinitely far upstream flow in the insulating channel region). The large difference in these two slip velocities makes the flow reversal occur over the left portion of the block. As a result, a pair of two counter vortexes is formed. In the limiting case of $\beta \to \infty$ as shown in Fig. 5(d), the induced zeta potential on the perfectly conductive surface is highest, and so is the Helmholtz-Smoluchowski velocity, resulting in the strongest pair of two counter-rotating vortices. At this situation, the liquid transportation in the vortices is several times faster than that in the insulating channel regions. This can be reflected from the values of stream function in the two vortex centers, which are 3.70 and −3.30, respectively.

Figure 6 shows the effect of the dimensionless natural zeta potential of the insulating microchannel walls on the flow patterns above a perfectly conductive block. For the case of $\bar{\zeta}_0 = -0.3$ shown in Fig. 6(a), a pair of counter-rotating vortices are formed due to a large difference between the induced zeta potential on the block surface and the natural zeta potential on insulating channel walls. When the natural zeta potential increases [as indicated in Fig. 6(b)], the vortex above the left side of the polarizable surface is gradually distorted, even disappears as shown in Fig. 6(c). In these two cases, the velocity of the incoming flow from upstream has

almost the same order of magnitude as the induced slip velocity on the left side of the polarizable surface. Thus, similar to the cases of Figs. 5(a) and 5(b), the flow reversal near the block centerline does not happen. However, on the right side of the polarizable surface, there always exists a negative induced Smoluchowski velocity, which counteracts with the incoming flow from upstream of the channel. Thus a vortex is present to fulfill the mass conservation. It is expected that the vortex on the right side of the block surface can disappear only when $\bar{\zeta}_0 \to -\infty$.

It should be noted that generation of this kind of microvortices is very useful. For example, the presence of vortical flow structure can enhance micromixing—which is always a challenging task because mixing in low Reynolds flows is intrinsically poor. Additionally, pumping and/or separating bioparticles [28–30] are also other potential applications.

ACKNOWLEDGMENTS

The authors gratefully acknowledge the financial support from the Ministry of Education of Singapore (Grant No. RG17/05) to C.Y.

[1] F. A. Morrison, J. Colloid Interface Sci. **34**, 210 (1970).
[2] S. S. Dukhin and V. N. Shilov, Colloid J. USSR **31**, 564 (1969).
[3] N. I. Gamayunov, V. A. Murtsovkin, and A. S. Dukhin, Colloid J. USSR **48**, 197 (1986).
[4] V. A. Murtsovkin, Colloid J. **58**, 341 (1996).
[5] T. M. Squires and M. Z. Bazant, J. Fluid Mech. **509**, 217 (2004).
[6] A. Ajdari, Phys. Rev. E **61**, R45 (2000).
[7] A. Ramos, H. Morgan, N. G. Green, and A. Castellanos, J. Colloid Interface Sci. **217**, 420 (1999).
[8] J. A. Levitan, S. Devasenathipathy, V. Studer, Y. Ben, T. Thorsen, T. M. Squires, and M. Z. Bazant, Colloids Surf., A **267**, 122 (2005).
[9] K. A. Rose, J. A. Meier, G. M. Dougherty, and J. G. Santiago, Phys. Rev. E **75**, 011503 (2007).
[10] S. Gangwal, O. J. Cayre, M. Z. Bazant, and O. D. Velev, Phys. Rev. Lett. **100**, 058302 (2008).
[11] M. Z. Bazant and Y. Ben, Lab Chip **6**, 1455 (2006).
[12] E. Yariv, Phys. Fluids **17**, 051702 (2005).
[13] D. Saintillan, E. Darve, and E. S. G. Shaqfeh, J. Fluid Mech. **563**, 223 (2006).
[14] F. C. Leinweber, J. C. T. Eijkel, J. G. Bomer, and A. Van Den Berg, Anal. Chem. **78**, 1425 (2006).
[15] C. K. Harnett, J. Templeton, K. A. Dunphy-Guzman, Y. M. Senousy, and M. P. Kanouff, Lab Chip **8**, 565 (2008).
[16] Z. Wu and D. Li, Electrochim. Acta **53**, 5827 (2008).
[17] N. Flores-Rodriguez and G. H. Markx, J. Phys. D **39**, 3356 (2006).
[18] T. M. Squires and S. R. Quake, Rev. Mod. Phys. **77**, 977 (2005).
[19] T. M. Squires and M. Z. Bazant, J. Fluid Mech. **560**, 65 (2006).
[20] D. T. Paris and F. K. Hurd, *Basic Electromagnetic Theory* (McGraw-Hill, New York, 1969).
[21] M. Z. Bazant, K. Thornton, and A. Ajdari, Phys. Rev. E **70**, 021506 (2004).
[22] G. Yossifon, I. Frankel, and T. Miloh, Phys. Fluids **18**, 117108 (2006).
[23] W. M. Deen, *Analysis of Transport Phenomena* (Oxford University Press, New York, 1998).
[24] L. Debnath and D. Bhatta, *Integral Transforms and their Applications* (Chapman and Hall, Boca Raton, 2007).
[25] A. Jeffrey, *Complex Analysis and Applications* (Taylor and Francis, Boca Raton, FL, 2006).
[26] M. Z. Bazant and T. M. Squires, Phys. Rev. Lett. **92**, 066101 (2004).
[27] G. Soni, T. M. Squires, and C. D. Meinhart, in *Proceedings of IMECE2007, ASME International Mechanical Engineering Congress and Exposition*, Seattle, Washington, USA, 2007 (unpublished).
[28] Y. K. Lee, L. M. Lee, W. L. W. Hau, and Y. Zohar, J. Microelectromech. Syst. **16**, 58 (2007).
[29] N. G. Green, Anal. Bioanal. Chem. **382**, 891 (2005).
[30] P. Takhistov, K. Duginova, and H. C. Chang, J. Colloid Interface Sci. **263**, 133 (2003).